Nanocrystalline superconducting islands of Nb_3Ge in a resistive grain boundary matrix with a bulk critical temperature of 12 K

2012 Supercond. Sci. Technol. 25 115014

(http://iopscience.iop.org/0953-2048/25/11/115014)

Supercond. Sci. Technol. **25** (2012) 115014 (7pp) doi:10.1088/0953-2048/25/11/115014

Nanocrystalline superconducting islands of Nb_3Ge in a resistive grain boundary matrix with a bulk critical temperature of 12 K

Elisabetta Pusceddu and Damian P Hampshire

Superconductivity Group, Centre for Materials Physics, Physics Department, Durham University, South Road, Durham DH1 3LE, UK

E-mail: d.p.hampshire@durham.ac.uk

Received 4 July 2012, in final form 23 August 2012
Published 25 September 2012
Online at stacks.iop.org/SUST/25/115014

Abstract

We report on nanocrystalline Nb_3Ge (A15) produced by hot isostatic pressing and annealing of milled material with a bulk critical temperature and bulk upper critical field of ~12 K and ~15 T respectively. Optimum macroscopic bulk critical values were only produced in a narrow window of processing parameters: mechanically alloyed $Nb_{0.75} + Ge_{0.25}$ milled for 6 or 20 h was processed in a hot isostatic press for 5 h operating at 2000 bar and 600 °C followed by annealing at 700 °C for 18 h. XRD data suggest that the crystalline components of both the optimum and non-optimum materials all have high Ge content, characteristic of Nb_3Ge material with a T_C of 15–17 K. In a small number of samples, very small zero-field screening signals were found at ~17 K that collapsed if a magnetic field of 0.5 T was applied. In contrast, high bulk-screening superconducting critical temperatures were accompanied by high bulk upper critical fields. We found that completely isolated nanocrystalline grains of Nb_3Ge would produce signals below the sensitivity of our commercial AC susceptometer and conclude that the nanocrystalline Nb_3Ge materials produced in this work with the highest superconducting critical properties consist of very weakly coupled islands of nanocrystalline material with critical temperatures up to ~17 K in a resistive grain boundary matrix which strongly couples the islands at ~12 K. We do not attribute the record critical bulk values obtained for Nb_3Ge, fabricated using solid-state processing alone, to improving the bulk crystalline properties but to improving the grain boundaries. Optimized nanocrystalline metallic superconductors produced by milling, HIP'ing and annealing have similarities with optimized high temperature and pnictide superconductors where improving and understanding the properties of the grain boundaries are key for improving their high field properties.

1. Introduction

Nanocrystalline superconducting materials are of interest both for technological applications [1, 2] and for fundamental studies of the mechanism of superconductivity since the fundamental length scales are comparable with the crystallite size [3]. Significant improvements in the upper critical field at zero temperature ($B_{c2}(0)$) have been discovered in nanocrystalline bulk superconductors primarily by converting microcrystalline powders into structurally disordered nanophase material through high-energy ball milling and then using compaction techniques involving hot isostatic pressing and annealing [2, 4–6]. This powder route processing also has the technologically important potential benefit that were it to produce markedly improved superconducting properties, nanocrystalline powders could easily be incorporated in the standard powder route processing used for both low temperature [7] and high temperature superconductors [8].

Although we have a basic understanding of why $B_{c2}(0)$ increases with decreasing the grain size on the nanoscale [6], we have no deep understanding of the spatial variation of the phonon density of states (assuming the superconductivity is phonon mediated), the electronic density of states and the scattering length across the crystalline grains and the grain boundaries of polycrystalline materials. Such information is required to understand the spatial variation of the superconducting properties and optimize high performance materials. We still largely rely on serendipity or empiricism (as is often the case for finding new superconductors) to identify new materials that in nanocrystalline form may provide high field superconductors or those established materials that when nanocrystalline may have a significantly increased range of field over which they can be used. This search for better materials is underpinned by the knowledge that nanocrystalline materials may also provide other improved properties such as increased strength and ductility, better phase stabilization and clean grain boundaries [9, 10]. This work on Nb_3Ge using dry powders, follows an earlier unsuccessful study using wet-milling in which no high field superconducting material was found [11]. In equilibrium, the A15(Nb_3Ge) structure only forms by a peritectic reaction at 1900 °C at (18 ± 1) at.% Ge [12] which is a demanding environment given that high superconducting critical properties require control of atomic diffusion [13, 14], compositional homogeneity and atomic ordering [15]. Quenched Nb_3Ge in thin film form shows the highest T_C (∼23 K) for the A15 superconducting compounds and a large $B_{C2}(0)$ of 38 T [16]. Splat cooling has produced tapes by rapid quenching from the molten state with T_C up to 17 K [17]. However conventional arc-melting and annealing techniques have only produced Nb_3Ge materials in bulk form with T_C values of up to 6–7 K [12, 18]. Here we investigate whether nanocrystalline Nb_3Ge, produced using only solid-state processing, has the potential to become an important material for high field applications.

2. Experimental details

A binary mixture of Nb (99.8%, −60 mesh, Alfa Aesar) and Ge (99.999%, −100 mesh, GoodFellow) powders of nominal composition $Nb_{0.75} + Ge_{0.25}$ was processed via high-energy ball milling (HEBM) for milling times up to 30 h using a dual-clamp SPEX 8000D mill and copper milling tools with a 4:1 ball to powder weight ratio. We chose copper as the milling media because copper has been found to enhance the formation of Nb_3Sn (and MgB_2) at low temperatures [19, 20] and its high thermal conductivity will lower any temperature increase during milling [9]. Furthermore, the binary alloy Cu–Nb phase diagram shows that no compound formation or intermediate phases occur between Cu and Nb and milling studies show that very little niobium dissolves in copper (or vice versa) [21]. Specially-designed copper vials were used and stored inside a glove box. All processing such as vial and ball coating and dislodging the powders from the inner walls and lid of the vial (which was done every 1 h throughout the milling process) was done inside the glove box which had an oxygen level less than 10 ppm. X-ray diffraction patterns (Cu Kα radiation) of the HEBM'ed powder initially showed peaks of a bcc-Nb rich solid solution $(Nb)_{ss}$, and a fcc-Ge rich solid solution $(Ge)_{ss}$. The principal $(Nb)_{ss}$ lines were significantly broadened and their intensity reduced with increased milling due to the progressive formation of a nanocrystalline disordered mixture [22]. Such mixtures are well established in the literature although a detailed TEM study would be required to determine the nature of the mixture at the nanoscale [23]. Figure 1 shows the average grain size (GS) and lattice parameters for the solid solutions of bcc-$(Nb)_{ss}$ and fcc-$(Ge)_{ss}$ at different milling stages obtained using the Rietveld method with TOPAS software. The increase in lattice parameter for the major phase $(Nb)_{ss}$ can be attributed to anti-site disorder whilst vacancy type defects can explain the decrease of the $(Ge)_{ss}$ unit cell [9]. The lattice parameter of $(Ge)_{ss}$ decreased and merged with that of $(Nb)_{ss}$ to produce a GS of ∼1 nm after about 11 h milling. The final equilibrium lattice constant (a_0) of ∼3.320 Å is higher than unmilled Nb (a_0 = 3.303 Å) by ∼0.6% which is consistent with the increase in lattice constant observed by Hellstern *et al* [13] of ∼1.2% for Nb–Al given the different milling procedures and the smaller atomic radius of Ge (152 pm) compared to that of Al (182 pm). The uncertainties in the grain size given in figure 1 (and table 1) are relatively large because these samples are not single phase, are nanocrystalline and the microstrain is not independently measured. If we make the assumption that there is no microstrain, we find an upper bound for the grain size after long milling of ∼6 nm, comparable to values found by other authors for similar milled alloys [6, 24] .

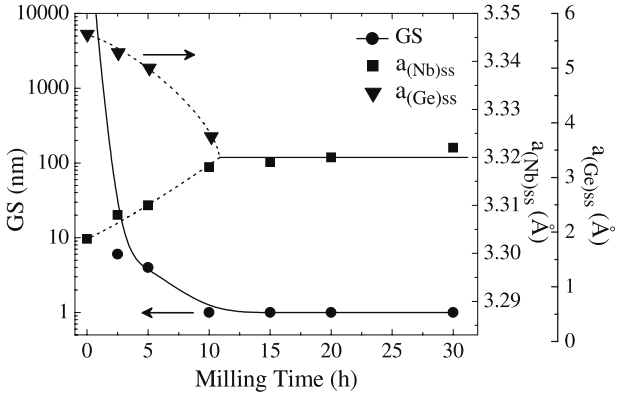

Figure 1. Grain size (GS) and lattice constant for solid solutions of $(Nb)_{ss}$ and $(Ge)_{ss}$ after milling.

Figure 2 shows the zero field AC magnetometry curves including the superconducting transition of the pressed Nb–Ge powders after different milling times. The data were collected using a Quantum Design AC magnetometer operating at 77 Hz with a small alternating field of ±10 Oe. The onset transition temperatures were found to be approximately 9 K because of the elemental niobium. Thereafter the large-signal transition was reduced to less than 5 K. Very sensitive magnetic susceptibility measurements show a general feature of milled Nb powder mixtures, namely

Table 1. Grain size (GS), A15 lattice parameter (a), critical temperature T_C and upper critical field $B_{c2}(0)$ for M6 and M20 processed using HIP600 + AZZZ and precursor material prior to annealing. The error bars for grain size are obtained from the Rietveld refinement. In square brackets, the onset critical transition temperature is recorded.

	Series M6				Series M20			
HIP600 + AZZZ	GS (nm)	a_{Nb-Ge} (Å)	T_C (K)	$B_{C2}(0)$ (T)	GS (nm)	a_{Nb-Ge} (Å)	T_C (K)	$B_{C2}(0)$ (T)
HIP600	2(1)	5.154(4)	8.0	1.0	2(1)	5.16(1)	7.4	1.0
HIP600 + A600	1(2)	5.155(2)	7.2 [17.0]	2.5	3(4)	5.157(4)	7.6 [16.4]	2.0
HIP600 + A700	2(7)	5.153(2)	12.0	15	8(6)	5.154(1)	10.8	14
HIP600 + A800	6(2)	5.154(2)	8.1	1.5	9(6)	5.154(2)	8.7	1.5
HIP600 + A900	11(5)	5.157(1)	7.8	1.5	11(8)	5.157(1)	8.1	1.5

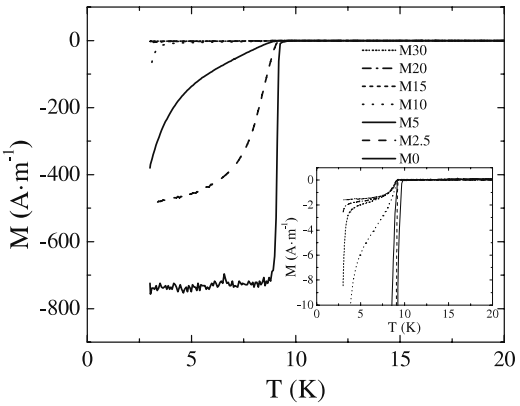

Figure 2. Zero field AC magnetometry curves for $Nb_{0.75} + Ge_{0.25}$ milled for up to 30 h.

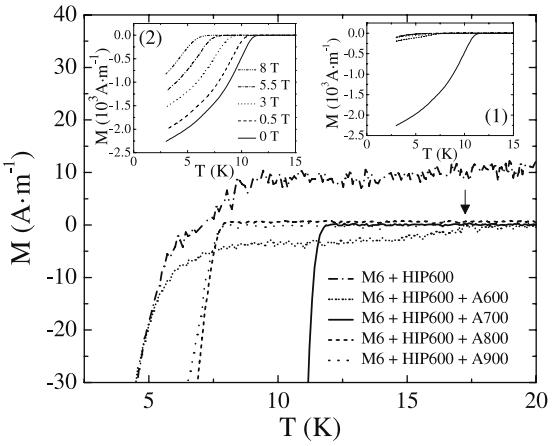

Figure 3. Zero-field magnetization $M(0, T)$ as a function of temperature for batch M6 + HIP600 + AXXX. Inset (1): full-scale y-axis zero-field magnetization data as a function of temperature for batch M6 + HIP600 + AXXX. Inset (2): in-field $M(B, T)$ for sample M6 + HIP600 + A700.

that there is always a very small signal with an onset temperature of 9 K about three orders of magnitude smaller than the signal obtained for full screening. One interpretation would be that the material is contaminated by microcrystalline Nb in all cases. However because of the prevalence of this small signal in materials produced in our laboratory and the lack of evidence for such contamination in XRD data, we attribute the signal to the pressed nanocrystalline materials. Two different types of milled powder were chosen for further processing: mixed phase, bcc structured material milled for 6 h (denoted M6) and disordered powder milled for 20 h (denoted M20). For each type of powder, four batches were produced, each of four bulk materials (32 samples in total). Powder samples were sealed in billets as follows: after milling, powders were transferred to a glove box and a few grams of powder were wrapped in a cylinder of niobium foil (0.025 μm thick, purity 99.8%, Alfa Aesar) and put into a stainless steel tube which had one end TIG (tungsten inert gas) welded. The other end was sealed using home-made apparatus which included an O-ring seal, isolation tap and a vacuum fitting. Subsequently the sealed tube was taken out of the glove box and the high purity argon enclosed was removed using a vacuum pump. A fly-press was then used to compress the tube and a spot welder used to complete the encapsulation of the sample inside the steel enclosure. The spot-welded end of the billet was then also TIG welded to improve the durability of the seal (particularly during HIP'ing). Eventually, after the relevant thermomechanical processing, the bulk sample was recovered by cutting open the billet. In the first batch, milled powders were pressed using a manually operated hydraulic press, sealed and annealed for 18 h at one of four temperatures (i.e. $A = 600$, 700, 800 and 900 °C) in high purity argon. In the second batch, powders were sealed and consolidated using the hot isostatic press (HIP) operating for 5 h at a pressure of 200 MPa at temperatures of 600, 700, 800 and 1200 °C in high purity argon. For the third and fourth batches of samples, bulk materials HIP'ed at 600 and at 1200 °C were given a second heat treatment at one of the four annealing temperatures for 18 h [25]. The properties of batch 3 are shown in table 1. We use a nomenclature below in which M6 + HIP600 + A700 denotes material produced by milling for 6 h followed by a HIP treatment at 600 °C × 5 h and then annealed at 700 °C × 18 h.

3. Results and analysis

Approximately cuboid bulk samples of ∼1 mm^3 volume were cut for superconducting property measurements. The AC magnetization $M(B, T)$ data were collected as a function of temperature (3 K $\leq T \leq$ 20 K) in dc magnetic fields up to 8 T. Figure 3 shows magnetization data for M6 + HIP600 and M6 + HIP600 + AXXX. The onset critical temperature (T_C) of M6 + HIP600 was 8.0 K increasing to a maximum value of 12.0 K at an optimum annealing

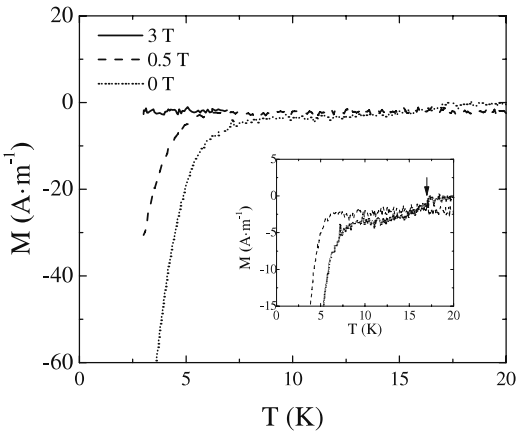

Figure 4. AC magnetization versus temperature for M6 + HIP600 + A600. The arrow shows the small signal in zero field at 17.0 K.

temperature of 700 °C. The presence of two superconducting transitions are shown for M6+HIP600+A600 at temperatures 7.2 and 17.0 K in figure 4. Six samples among the thirty two, found only among those batches that include the annealing process showed these double transitions with the higher T_C above 16 K. These small-signal higher temperature transitions, close to the detection limit for our equipment, disappeared (were not detectable) in magnetic fields of 0.5 T. This suggests that these granular samples consist of isolated regions of high-T_C which only weakly couple across resistive regions in-field, reminiscent of the weak-link problem in high temperature and pnictide superconductors and associated with grain boundaries [26–28]. Isolated regions of highly-ordered metastable A15 grains (whose size is smaller than the coherence length) have been reported before [3, 29]. Critical temperature values of >16 K are of note, since they are similar to those found using splat cooling [17]. We also note a small paramagnetic magnetization in the normal state of precursor powders and batch 2, that annealing removes. Inset (1) of figure 3 shows all the zero-field magnetization data for M6+HIP600+AXXX. The large saturation magnetization shown by M6 + HIP600 + A700 at low temperatures in zero field is accompanied by large macroscopic screening currents in-field. Among the thirty two samples, just two show the very high bulk critical parameters with macroscopic screening currents flowing in high fields above 2 T at low temperatures—M6 + HIP600 + A700 and M20 + HIP600 + A700—although in neither of these could we detect the small-signal high-T_C transitions. Inset (2) of figure 3 shows the in-field response produced by M6 + HIP600 + A700 up to 8 T where $T_C \sim 12.0$ K and $B_{C2}(0) \sim 15$ T. The critical parameters for the equivalent unannealed sample M6+HIP600 were only 8.0 K and 1 T. The convex curvature of $B_{C2}(T)$ near T_C, can be attributed to a distribution in T_C so where several in-field data points were measured, the zero-field datum was not included in determining $B_{C2}(0)$. We have calculated $B_{C2}(0)$ by using the onset of the diamagnetic signal to characterize the superconducting transition, linearly extrapolating the $B_{C2}(T)$ data to zero temperature and citing 69% of this extrapolated value following WHH theory [30]. For the high critical parameter samples, if we calculate $B_{C2}(0)$ using only data at 0.5 and 3 T, $B_{C2}(0)$ is about 10% higher than the values shown in table 1 (which are rounded to the nearest 0.5 T). Similarly, M20 + HIP600 + A700 showed a large enhancement of both T_C and $B_{C2}(0)$ from 7.4 K and 1 T (for M20 + HIP600) to 10.8 K and 14 T.

Microstructure and compositional phases were probed using a Hitachi SU-70 FEG-SEM equipped with an Oxford Instrument INCA energy dispersive x-ray (EDX) system to obtain chemical analysis on the scale of ∼0.2 μm. Most samples show large areas of porous material due to the well-known poor workability of Ge. EDX results for samples M6 + HIP600 and M6 + HIP1200 show a large average Cu content of ∼9 at.% but with a very different spatial distribution of the Cu between these two samples. Sample M6 + HIP600, processed at temperature below Ge (938.3 °C), Cu (1084.6 °C) and $Cu_{64}Ge_{36}$ (640 °C) melting points, displays very non-uniform distribution of Cu with most of the copper appearing in large regions of almost pure copper as well as some Cu–Ge regions. In contrast, M6 + HIP1200 exhibits an almost uniform distribution of Cu throughout the sample. The copper content comes from the milling media. The content could be reduced using harder milling media such as tungsten carbide or ceramic media. The EDX data and the XRD data (considered below), confirms that the majority phases observed in both samples are Nb_3Ge, Nb_5Ge_3, and terminal solid solutions $(Nb)_{ss}$ and $(Cu)_{ss}$.

X-ray diffraction patterns were measured for all samples and similar behaviour found for batches 1–3. The precursor powder exhibited a structurally disordered (and metastable) phase [14] with broad overlapping peaks. The number and intensity of XRD peaks significantly increased with increasingly aggressive heat treatments along with a progressive reduction of peak widths due a continuous GS growth from about 2 up to 11 nm. The amount of crystalline Nb_3Ge and Nb_5Ge_3 gradually increases from the lowest temperatures whilst NbO and GeO_2 crystallization only produces significant XRD peaks at temperatures higher than 700 °C. Hence despite the very considerable care to minimize oxygen contamination using the glove box during all the processing, the very high reactivity of the nanocrystalline powders has lead to a measurable incorporation of oxygen in the final bulk materials (which may also play a role in the paramagnetic signals observed). In contrast to batches 1–3, XRD data for batch 4 (M6 + HIP1200 + AXXX and M20 + HIP1200+AXXX) showed the final anneal did not change the number and the intensity of peaks as the crystalline structures were already well developed in the precursor samples M6 + HIP1200 and M20 + HIP1200.

Figure 5 shows the correlation between bulk T_C and the A15 phase lattice constant derived from the XRD data using the Rietveld refinement for batch 3—M6 + HIP600 + AXXX and M20 + HIP600 + AXXX. Figure 6 shows the onset critical temperature and A15 lattice constants for batches 2 and 3 as well as equivalent data estimated from sputtered Nb_3Ge material from the literature [12]. The lattice constant of the crystalline Nb_3Ge A15 phase in all our bulk samples is characteristic of T_Cs values of 15–17 K in films [31]. Despite

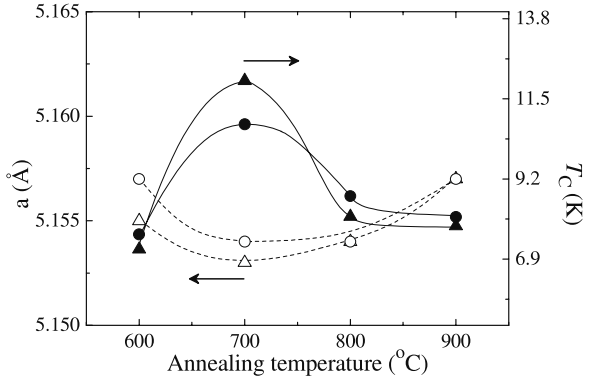

Figure 5. Bulk critical temperature (full symbol) and lattice constant (empty symbol) for the A15 structure in M6 + HIP600 + AXXX (triangle) and M20 + HIP600 + AXXX (circle).

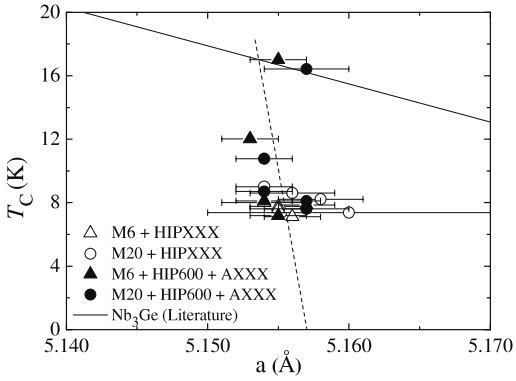

Figure 6. Onset critical temperature versus lattice constant for the A15 structure in batches 2 and 3—samples M6 + HIPXXX (open triangle), M20 + HIPXXX (open circle), M6 + HIP600 + AXXX (closed triangle) and M20 + HIP600 + AXXX (closed circle). The solid line is data from the literature for Nb_3Ge films [31].

this, all bar the two optimum samples have low bulk T_C and low bulk $B_{C2}(0)$ consistent with poor connectivity between the grains.

4. Discussion

In granular superconducting materials, the ratio of the susceptibility of a collection of completely decoupled spherical grains which together form a macroscopic spherical sample to that of the susceptibility from full screening ($\frac{\chi'_{\text{granular}}}{\chi'_{\text{bulk}}}$) in the limit that the London penetration depth λ_L is much less than the radius (a) of the spherical grains, is given by [32]

$$\frac{\chi'_{\text{granular}}}{\chi'_{\text{bulk}}} = \left[1 - \frac{3\lambda_L}{a}\right] \qquad \text{for } \lambda_L \ll a. \tag{1}$$

Schoenberg [33, 34] has provided a general solution for the ratio in equation (1). With increasing λ_L/a, the susceptibility ratio rapidly changes to the limiting expression for a large penetration depth [32, 34] so that once the penetration depth is larger than a we have:

$$\frac{\chi'_{\text{granular}}}{\chi'_{\text{bulk}}} \approx \frac{1}{15}\frac{a^2}{\lambda_L^2} \qquad \text{for } \lambda_L > a, \tag{2}$$

which is further reduced by the factor a/ξ_{BCS} when $a < \xi_{BCS}$, to account for non-local electrodynamics [35] where ξ_{BCS} is the BCS coherence length [36] . From the data in figure 2, we find $\frac{\chi'_{\text{granular}}}{\chi'_{\text{bulk}}} \approx 2 \times 10^{-3}$. If we attribute the small signal found after 30 h milling to completely decoupled nanocrystalline Nb and use $\lambda_L = 52$ nm and $\xi_{BCS} = 35$ nm, even for an upper bound grain size (i.e. no microstrain) of 6 nm, equation (2) gives a calculated value of $\sim 2 \times 10^{-4}$—an order of magnitude smaller than the experimental signal. Equally for the Nb_3Ge, the experimental value (figure 4) is again $\sim 2 \times 10^{-3}$ whereas the theoretical value with a grain size of 6 nm and $\lambda_L = 90$ nm [37] gives an (upper bound) theoretical value of 3×10^{-4} . This value is calculated assuming there is no reduction from electrodynamic effects (note that for Nb_3Sn [38], $\xi_{BCS} \sim 4$ nm) and that the samples are entirely the A15 phase. We conclude that these signals, close to the detection limit for our equipment, are therefore too large to be predominantly associated with intragranular currents. There must be significant coupling across the grain boundaries so that Josephson screening currents circulate beyond the nanoscale. Consistent with the sensitivity of Josephson currents to magnetic fields, the zero-field signal disappears in high fields. In the context of this discussion, the XRD data show that the crystalline material in the nanocrystalline grains of many of our samples has high Ge content with T_C of 15–17 K so the nanocrystalline intragranular signal they produce could simply be below our detection limit. The small signal high T_C values that are observed in some samples occur because of a combination of (relatively) high sensitivity measurements and good grain boundaries. The grain boundary matrix is sufficiently high resistivity material that significant current densities only flow across them in zero field at 17 K. Eventually at sufficiently low temperatures, the coherence length in the normal grain boundary material (ξ_N) [39–41] becomes sufficiently long to couple the grains. The grain boundaries are sufficiently low resistivity that the record bulk values reported here are eventually achieved in the optimum samples at 12 K. Finally we note the similarities between the optimum nanocrystalline materials reported here and high temperature (HTS) and pnictide superconductors. Grain boundaries acting as weak-links have been a long-standing problem for these materials and the structure and local properties remain a source of much study [27, 28, 42–44]. Whether the approach used here could be useful for improving HTS/pnictide materials or whether the approach used with HTS materials where all high-angle grain boundaries are removed (and intragranular pinning sites inserted) could be useful for improving any of the low temperature superconductors remain open questions.

5. Conclusion

We report that milling and HIP'ing can be used to produce islands of crystalline Nb_3Ge A15 material of high Ge

content with high bulk critical parameters separated by a resistive grain boundary matrix. Good connectivity across the grain boundaries is only produced in a narrow window of processing at low temperatures before the oxides crystallize and the copper disperses—processes that may compete with intergranular superconductivity. Since all the materials were multiphase with copper and oxygen contamination, more improvements may still be expected. Significantly higher sensitivity susceptibility measurements are required for measuring intragranular currents in nanocrystalline materials. They may provide useful information about the temperatures and fields at which the nanoscale components of nanocrystalline materials become superconducting and hence help in the search for new high field superconductors.

Acknowledgments

The authors thank Professor J S O Evans for access to the XRD facility. This work was supported by the Sardinian Regional Agency for Work under grant no. MAB 2.2 2005-169 Prot. N10162 and EPSRC.

References

[1] Niu H J and Hampshire D P 2003 Disordered nanocrystalline superconducting $EPbMo_6S_8$ with very large upper critical field *Phys. Rev. Lett.* **91** 027002
[2] Hampshire D P and Niu H J, International patent number WO03/094251-A2-2002
[3] Mondal P, Manekar M, Kumar R, Ganguli T and Roy S B 2008 Superconducting properties of nanocrystalline Nb_3Al in Nb–Al matrix *Appl. Phys. Lett.* **92** 052507
[4] Niu H J and Hampshire D P 2004 Critical parameters of disordered nanocrystalline superconducting Chevrel phase $PbMo_6S_8$ *Phys. Rev.* B **69** 174503
[5] Cooley L D, Hu Y F and Moodenbaugh A R 2006 Enhancement of the upper critical field of Nb_3Sn utilizing disorder introduced by ball milling the elements *Appl. Phys. Lett.* **88** 142506
[6] Taylor D M J, Al-Jawad M and Hampshire D P 2008 A new paradigm for fabricating bulk high-field superconductors *Supercond. Sci. Technol.* **21** 125006
[7] Elen J D, van Beijnen C A M and van der Klein C A M 1977 Multifilament V_3Ga and Nb_3Sn superconductors produced by the ECN-technique *IEEE Trans. Magn.* **13** 470–3
[8] Hikata T, Sato K and Hitotsuyanagi H 1989 Ag-sheathed Bi–Pb–Sr–Ca–Cu–O superconducting wires with high critical current density *Japan. J. Appl. Phys.* **28** 82
[9] Suryanarayana C 2001 Mechanical alloying and milling *Prog. Mater. Sci.* **46** 1–184
[10] Lu K 1996 Nanocrystalline metals crystallized from amorphous solids: nanocrystallization, structure, and properties *Mater. Sci. Eng.* R **16** 161–221
[11] Pusceddu E, Charlton S and Hampshire D P 2008 Nanocrystalline Nb–Al–Ge mixtures fabricated using wet mechanical milling *J. Phys.: Conf. Ser.* **97** 012241
[12] Jorda J L, Flükiger R and Muller J 1978 The phase diagram of the niobium–germanium system *J. Less-Common Met.* **62** 25
[13] Hellstern E, Schultz L, Bormann R and Lee D 1988 Phase formation in mechanically alloyed Nb–Al powders *Appl. Phys. Lett.* **53** 1399
[14] Chatterjee P P, Pabi S K and Manna I 1999 An allotropic transformation induced by mechanical alloying *J. Appl. Phys.* **86** 5912
[15] Willens R H *et al* 1969 Superconductivity of Nb_3Al *Solid State Commun.* **7** 837–41
[16] Foner S, McNiff E J Jr, Gavaler J R and Janoko M A 1974 Upper critical fields of Nb_3Ge thin film superconductors *Phys. Lett.* A **47** 485
[17] Evetts J (ed) 1992 *Concise Encyclopedia of Magnetic and Superconducting Materials* (Oxford: Pergamon)
[18] Matthias B T, Geballe T H, Willens R H, Corenzwit E and Hull G W 1965 Superconductivity of Nb_3Ge *Phys. Rev.* A **139** 1501
[19] Lefranc G and Müller A 1976 Effect of copper additions on superconducting niobium–tin sintered material *J. Less-Common Met.* **45** 339–42
[20] Varghese N *et al* 2011 Influence of nano-Cu additive on MgB_2 phase formation, processing temperature, and transport properties *J. Appl. Phys.* **109** 033902
[21] Botcharova E, Freudenberger J and Schultz L 2004 Cu–Nb alloys prepared by mechanical alloying and subsequent heat treatment *J. Alloys Compounds* **365** 157–63
[22] Di L M and Bakker H 1992 Atomic disorder induced by mechanical milling in the Nb_3Au intermetallic compound *J. Appl. Phys.* **71** 5650–3
[23] Huang B, Perez R, Lavernia E and Luton M 1996 Formation of supersaturated solid solutions by mechanical alloying *Nanostruct. Mater.* **7** 67–9
[24] Rock C and Okazaki K 1995 Detailed phase analysis of a 77 at.% Nb–Al system prepared by low-energy ball milling *Nanostruct. Mater.* **5** 643–56
[25] Flükiger R, Spitzkli P, Heiniger F and Muller J 1969 Annealling conditions and superconducting behaviour of Nb-based A15-type compounds *Phys. Lett.* A **29** 407
[26] Dimos D, Chaudhari P and Mannhart J 1990 Superconducting transport properties of grain boundaries in $YBa_2Cu_3O_7$ bicrystals *Phys. Rev.* B **41** 4038–49
[27] Durrell J H *et al* 2011 The behaviour of grain boundaroes in the Fe-based superconductors *Rep. Prog. Phys.* **74** 124511
[28] Hilgenkamp H and Mannhart J 2002 Grain boundaries in high-T_c superconductors *Rev. Mod. Phys.* **74** 485–549
[29] Tanabe K, Asano H and Michikami O 1984 Josephson properties of Nb_3Ge/oxide/Pb tunnel junctions *Appl. Phys. Lett.* **44** 559
[30] Werthamer N R, Helfand E and Hohenberg P C 1966 Temperature and purity dependence of the superconducting critical field, H_{C2}. III. Electron spin and spin–orbit effects *Phys. Rev.* **147** 295–302
[31] Rogowski D A and Roy R 1976 Composition versus a_0 and T_c relations in superconducting Nb_3Ge thin films *J. Appl. Phys.* **47** 4635–42
[32] May R M and Schafroth M R 1959 Susceptibility of superconducting spheres *Proc. Phys. Soc.* **74** 153
[33] Shoenberg D 1952 *Superconductivity* (Cambridge: Cambridge University Press)
[34] Broun D M and Huttema W A 2009 Effective magnetic penetration depth in superconducting cylinders and spheres with highly anisotropic electrodynamics *Phys. Rev.* B **79** 094527
[35] Tinkham M 1996 *Introduction to Superconductivity* 2nd edn (Singapore: McGraw-Hill)
[36] Bardeen J, Cooper L N and Schrieffer J R 1957 Theory of Superconductivity *Phys. Rev.* **108** 1175–204
[37] Poole C P 2000 *Handbook of Superconductivity* 1st edn (New York: Academic)
[38] Deutscher G and Bok J 1993 Short coherence length superconductors and the Fermi velocity paradox *Chin. J. Phys.* **31** 805

[39] Schmid A A 1966 Time dependent Ginzburg–Landau equation and its application to the problem of resistivity in the mixed state *Phys. Kondens. Materie* **5** 302–17

[40] Hu C-R and Thompson R S 1972 Dynamic structure of vortices in superconductors, $H \ll H_{c2}$ *Phys. Rev.* B **6** 110–20

[41] Carty G and Hampshire D P 2008 Visualising the mechanism that determines the critical current density in polycrystalline superconductors using time-dependent Ginzburg–Landau theory *Phys. Rev.* B **77** 172501

[42] Larbalestier D *et al* 1987 Experiments concerning the connective nature of superconductivity in $YBa_2Cu_3O_7$ *J. Appl. Phys.* **62** 3308

[43] Lang K M *et al* 2002 Imaging the granular structure of high-T_c superconductivity in underdoped $Bi_2Sr_2CaCu_2O_{8+\delta}$ *Nature* **415** 412–6

[44] Weiss J D *et al* 2012 High Intergrain critical current density in fine-grain $(Ba_{0.6}K_{0.4})Fe_2As_2$ wires and bulks *Nature Mater.* **11** 682–5